

Type Ia supernovae within dense carbon-oxygen rich envelopes: a model for ‘Super-Chandrasekhar’ explosions?

U. M. Noebauer,^{1*} S. Taubenberger,^{1,2} S. Blinnikov,^{3,4,5} E. Sorokina,^{3,4,6}
and W. Hillebrandt¹

¹*Max-Planck-Institut für Astrophysik, Karl-Schwarzschild-Str. 1, D-85748 Garching, Germany*

²*European Southern Observatory, Karl-Schwarzschild-Str. 2, D-85748 Garching, Germany*

³*Institute for Theoretical and Experimental Physics (ITEP), 117218 Moscow, Russia*

⁴*Kavli Institute for the Physics and Mathematics of the Universe (WPI), The University of Tokyo, Kashiwa, Chiba 277-8583, Japan*

⁵*All-Russia Research Institute of Automatics (VNIIA), 127005 Moscow, Russia*

⁶*Sternberg Astronomical Institute, M.V.Lomonosov Moscow State University, 119991 Moscow, Russia*

Accepted XXX. Received YYY; in original form ZZZ

ABSTRACT

We investigate the consequences of fairly normal Type Ia supernovae being embedded in compact and dense envelopes of carbon and oxygen rich circumstellar material by means of detailed radiation hydrodynamic simulations. Our main focus rests on exploring the effects of the interaction between ejecta and circumstellar material on the ejecta evolution and the broad-band light curve. In our calculations, we find that a strong reverse shock efficiently decelerates and compresses the ejecta material. This leads to a significant broadening of the optical light curve, a longer rise to maximum and a slower decline in the tail phase. During the interaction, substantial radiative energy is generated, which mostly emerges in the extreme ultraviolet and X-ray regime. Only if reprocessing due to radiation–matter interactions is very efficient, a significant boost in the optical light curve is observed. We discuss these findings in particular in the context of the super-luminous event SN 2009dc. As our calculations are able to reproduce a number of its peculiar properties, we conclude that the flavour of the interaction scenario investigated in this work constitutes a promising candidate to explain such ‘Super-Chandrasekhar’ supernovae.

Key words: hydrodynamics – radiative transfer – circumstellar matter – supernovae: general – supernovae: individual: SN 2009dc

1 INTRODUCTION

The presence of circumstellar material (CSM) is playing an ever more important role for the understanding of supernova (SN) evolution. For example, the interplay between CSM and the SN ejecta can be crucial for shaping some of the defining properties for particular SN classes. Prominent examples in this context are Type IIn supernovae (SNe IIn). Here, the eponymous narrow line features (Schlegel 1990) are ascribed to the presence of a dense CSM envelope, in which hydrogen recombines (e.g. Chugai et al. 2004). The presence of substantial amounts of CSM is also often invoked as a possible explanation for the intense luminosity of some of the most powerful SN events (e.g. Ofek et al. 2007; Chevalier & Irwin 2011), which are typically referred to as super-luminous SNe. In this scenario, the vast kinetic energy pool of the ejecta may be tapped through the shock

heating processes in the ejecta–CSM interaction, converted partially to thermal and radiation energy and thus power the intense light output of such systems (see, for example, the ejecta–CSM interaction calculation for the super-luminous SN PTF12dam by Baklanov et al. 2015). Note, however, that in the context of super-luminous SNe, also other models, such as the pair-instability mechanism (e.g. Barkat et al. 1967; Gal-Yam et al. 2009) or the magnetar-powered scenario (e.g. Kasen & Bildsten 2010; Nicholl et al. 2013), are heavily discussed. The increasing relevance of ejecta–CSM interaction is also owed to the success of modern survey programmes in catching SNe at ever earlier phases (e.g. Gal-Yam et al. 2014). During these epochs, right after the explosion, the observables probe the immediate vicinity of the explosion site. Any interaction with CSM at these times imprints characteristic features onto spectra and the early light curves (see, for example, systematic exploration in the SNe Ia context by Piro & Morozova 2016). Interpret-

* unoebauer@mpa-garching.mpg.de

ing these, gives insights into the mass-loss history of the progenitor system and thus into the exploding object.

In recent years, an increasing number of observations has revealed CSM interaction signatures in Type Ia supernovae (SNe Ia) as well, which are associated with the complete thermonuclear incineration of a carbon-oxygen white dwarf (WD). A prominent examples was PTF11kx (Dilday et al. 2012), which exhibits multiple CSM shells in its immediate environment, but many more strongly interacting SNe Ia have been identified (see, for example, census by Silverman et al. 2013). In addition to the direct observational evidence, the presence of CSM is invoked as a potential explanation for a class of SNe Ia, which often exhibit extraordinary luminosities. These events, commonly dubbed ‘Super-Chandrasekhar’ explosions (Howell et al. 2006), of which SN 2009dc (Yamanaka et al. 2009; Silverman et al. 2011; Taubenberger et al. 2011) is the prototype, elude an explanation within the standard Chandrasekhar-mass explosion paradigm.

In light of the relevance of the interplay between SN Ia ejecta and its circumstellar environment, we perform detailed radiation hydrodynamical calculations of interacting SNe Ia in this work. Conceptually similar explorations have been performed by Khokhlov et al. (1993); Nomoto et al. (2005); Fryer et al. (2010); Blinnikov & Sorokina (2010). However, we focus here on a specific realisation of the interaction scenario, which draws inspiration from previous investigations of the ejecta–CSM interplay in the context of super-luminous SNe Ia (Taubenberger et al. 2013). In particular, we consider fairly normal SNe Ia occurring within a dense carbon and oxygen rich envelope and examine the consequences of the ensuing ejecta–CSM interaction for the overall evolution of the system and its energy output. Apart from determining the generic evolution of these interaction models, an important aspect of this work lies in exploring whether this scenario provides a plausible explanation for Super-Chandrasekhar SNe Ia.

We begin this study by briefly reviewing some key aspects of super-luminous SNe Ia in Section 2. This is followed by a detailed overview of the investigated models and the used numerical tool in Section 3. The results of our simulations, which are presented and compared with observations of super-luminous SNe Ia in Section 4, will be discussed in detail in Section 5.

2 SUPER-CHANDRASEKHAR SUPERNOVAE

2.1 General Properties

We briefly review some of the important characteristics of a sub-class of thermonuclear supernovae of which we consider SN 2009dc the prototype. All objects in this sub-class share some distinct features which set them apart from ‘normal’ Type Ia explosions, used in cosmological studies. However, within the members of this group a sizeable spread in their properties persists, leading to quite a non-homogeneous class, which we refer to as ‘Super-Chandrasekhar’ objects.

Considering the photometric appearance, the most striking feature of the Super-Chandrasekhar objects is their high to outstanding peak luminosity, surpassing the intrinsic maximum brightness of normal SNe Ia by factors up to two (Howell et al. 2006; Scalzo et al. 2010;

Yuan et al. 2010). In addition to the high luminosity, the Super-Chandrasekhar objects show a broad and slowly declining light curve with a typical $\Delta m_{15}(B) \sim 0.6 - 1$ (Scalzo et al. 2010; Taubenberger et al. 2011). The light curve rise to its peak seems to progress slowly, in particular in the case of SN 2009dc, for which a very early detection has determined a lower rise time limit, $t_{\text{rise}} \geq 23$ d (Silverman et al. 2011). After maximum, the Super-Chandrasekhar objects exhibit a generically slower decline during the tail phase than normal SNe Ia (e.g. Taubenberger et al. 2013). However, at least in a number of objects, SN 2006gz (Maeda et al. 2009), SN 2009dc (Silverman et al. 2011; Taubenberger et al. 2011) and possibly SN 2012dn (Chakradhari et al. 2014), a prominent break in the late light curve evolution has been observed, which is often attributed to the onset of dust formation (Maeda et al. 2009; Taubenberger et al. 2011; Nozawa et al. 2011; Taubenberger et al. 2013). For SN 2009dc, this occurred around $t \sim 200$ d (Taubenberger et al. 2011).

The group of Super-Chandrasekhar objects not only differs from normal SNe Ia in terms of its photometric behaviour but it also shows a number of characteristic spectral peculiarities. Typically, the spectral energy distribution (SED) of these objects peaks at bluer wavelengths than expected for normal SNe Ia during early phases (Brown et al. 2014). Related to this, the absorption troughs of prominent P-Cygni lines, in particular of Ca II and Si II, are not very deep which may be interpreted as an indication for an underlying continuum contribution (Hachinger et al. 2012). Contrary to normal SNe Ia for which carbon lines are typically weak and only observed during the early phases, such lines appear much stronger and persist also until later times in the Super-Chandrasekhar class (e.g. Taubenberger et al. 2011; Chakradhari et al. 2014). Finally, the line velocities, of important SN Ia lines, as measured by the blue shift of the location of maximum absorption, exhibit a peculiar behaviour: in SN 2009dc, these velocities are consistently lower than in normal SNe Ia (Yamanaka et al. 2009; Silverman et al. 2011; Taubenberger et al. 2011). However, a complementary behaviour may also be observed in this class: the less luminous members, such as SN 2006gz (Hicken et al. 2007) and SN 2012dn (Chakradhari et al. 2014), show typically line velocities which are much closer to those observed in normal SNe Ia.

2.2 Proposed Models

Many of the peculiar properties listed above challenge the canonical theoretical model for SNe Ia. In particular, the high intrinsic luminosity of the Super-Chandrasekhar objects stands in contrast to the standard interpretation, in which the light output from SNe Ia is solely attributed to the energy released in radioactive decay reactions. A number of theoretical scenarios have been discussed in the literature to address this discrepancy. In general, these models may be divided into two groups: one attempts to reconcile these events with the standard radioactivity picture by exploring mechanisms to increase the stability limit of white dwarfs. In contrast to that, approaches of the second group search for additional energy sources, which may contribute to the light output in these super-luminous events.

In general, a nickel mass of $M_{\text{Ni}} \approx 1.8 M_{\odot}$ is needed

to explain the peak luminosity of SN 2009dc solely with the energy release from radioactivity (Yamanaka et al. 2009; Silverman et al. 2011; Taubenberger et al. 2011). Synthesising that amount of radioactive material during the thermonuclear burning phase would in turn require an even higher total mass of the progenitor white dwarf. Taubenberger et al. (2011) estimate an ejecta mass of the order of $M_{\text{ej}} \approx 2.8 M_{\odot}$, which clashes with the classical Chandrasekhar mass, the stability limit of a degenerate electron gas. One possibility to overcome this limit is to invoke rotation. A rapidly rotating WD may reach masses up to $\sim 2.1 M_{\odot}$ (Yoon & Langer 2005). Detailed numerical simulations (Pfannes et al. 2010a,b) have demonstrated that pure detonations may efficiently incinerate such heavily rotating white dwarfs, producing large amounts of radioactive nickel. However, the intense thermonuclear burning leads to high kinetic energies in the ejecta and iron group and intermediate mass elements being located at rather high velocities, contrary to what is observed. Moreover, even in the very extreme case investigated by (Kamiya et al. 2012), in which rotating WD models with $M = 2.8 M_{\odot}$ have been constructed, the light curve peak of SN 2009dc could only be reproduced after neglecting host galaxy extinction. In a complementary scenario (suggested for example by Howell et al. 2006; Hicken et al. 2007), the classical stability limit is overcome by considering the merger of two heavy (possibly rotating) WDs. The total mass of the system may then again easily surpass the Chandrasekhar limit.

In addition to the problems of the Super-Chandrasekhar scenario identified in detailed numerical simulations, Taubenberger et al. (2013) presented compelling arguments against any model which attempts to explain the SN 2009dc-like objects by radioactivity alone. Ignoring the detailed processes which could lead to the production of very high nickel masses, they showed that the bolometric light curve of an explosion with a nickel mass of $M_{\text{Ni}} = 1.6 M_{\odot}$ and an ejecta mass consistent with the observed kinematics, $M_{\text{ejecta}} = 3.0 M_{\odot}$, as suggested by Hachinger et al. (2012), matches the observed peak luminosity of SN 2009dc but fails to reproduce the tail region owing to the increased trapping of γ and optical radiation. Additionally, the recent study by Dhawan et al. (2016), which aims at deriving nickel masses from infrared data, did not find any indications for extraordinarily high nickel masses for the Super-Chandrasekhar objects SN 2007if and SN 2009dc.

A completely different view of the problem of Super-Chandrasekhar SNe Ia is taken by the interaction scenario (see specifically Hachinger et al. 2012; Taubenberger et al. 2013). Here, no extraordinarily high nickel masses are required. Instead, an additional energy source in the form of interactions between the ejecta and some form of CSM is invoked, which, together with the energy release due to radioactivity, is suggested to power the light curve of Super-Chandrasekhar SNe, very similar to what is discussed in the context of other super-luminous supernovae (e.g. Ofek et al. 2007; Chevalier & Irwin 2011). In this scenario, kinetic energy of the supernova ejecta is converted into radiation and thermal energy in shock heating processes during the interaction with the CSM. Already tapping a small fraction of the kinetic energy pool of the SN ejecta could be sufficient to explain the intense luminosities of Super-Chandrasekhar objects. However, the plausibility of the interaction scenario

as the mechanism underlying Super-Chandrasekhar objects is challenged by the lack of clear and unambiguous interaction signatures, such as narrow emission lines, as in the case of Type II supernovae, in the observational data.

Despite this, Taubenberger et al. (2013) could construct a simple toy model with which the tail light curve of SN 2009dc could be well reproduced simply by assuming an overall increase in ejecta density, thought to be the result of shock compression processes. However, being a pure radiative transfer investigation no definitive statement about the peak of the light curve and whether ejecta–CSM interaction could provide the requested luminosity boost could be made.

3 MODELS AND USED METHODS

In this work, we consider ejecta of fairly normal SN Ia explosions and embed them into a compact and dense carbon-oxygen CSM environment. Using a sophisticated radiation hydrodynamical code, we follow the evolution of these configurations and examine the exact consequences of the interaction between the SN ejecta and the CSM. In particular, we focus on kinematic changes within the ejecta and the effects on the optical light curve.

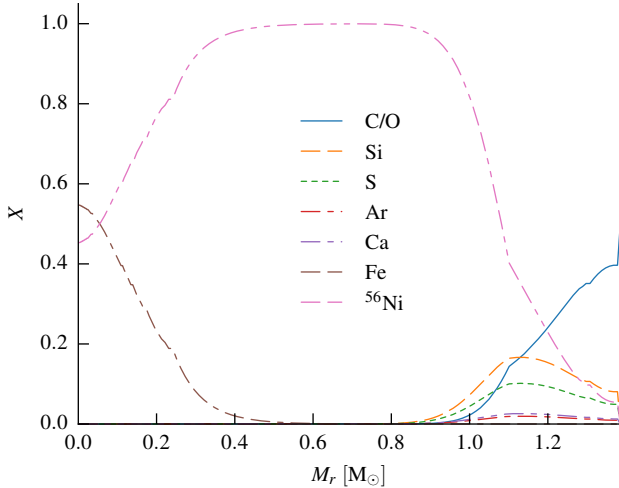
In the choice of model parameters, we draw inspiration from the investigation of Taubenberger et al. (2013). Relying on similar parameters, we may, in addition to studying the generic consequences of ejecta–CSM interaction, also examine whether such a scenario provides a viable explanation for Super-Chandrasekhar SNe. By construction, the particular flavour of ejecta–CSM interaction studied in this work addresses the common criticism voiced against the interactions scenario in this context, namely the absence of any clear unambiguous interaction signatures in the observational data of Super-Chandrasekhar objects. With the restriction to compact, carbon and oxygen rich CSM configurations, the non-detection of narrow hydrogen or helium emission lines would be a natural consequence of the absence of these elements in the CSM. Due to the small extent of the CSM, the interaction phase, during which the ejecta continuously sweeps up the material, would be quite brief. Consequently, other interaction signatures, such as high UV fluxes, would be restricted to the early phases of the supernova evolution, which are typically not very well observed. Such a circumstellar environment could emerge in the context of the classical double degenerate scenario (Webbink 1984), in which the complete disruption of the secondary WD during the merger does not induce an explosion but eventually the ensuing accretion process of the material onto the primary WD (c.f. Yoon et al. 2007). More details on the link between this ‘slow-merger’ scenario and the CSM configurations investigated here are provided in Section 5.1. In the following, we describe our input model and briefly review the numerical tool with which the calculations are performed, before presenting our results.

3.1 Ejecta–CSM Models

Taubenberger et al. (2013) could successfully reproduce the tail light curve of SN 2009dc in a pure radiative transfer calculation using a simple toy model, referred to as

Table 1. Main properties of the ejecta model m100101, produced by Woosley et al. (2007) and used in our study.

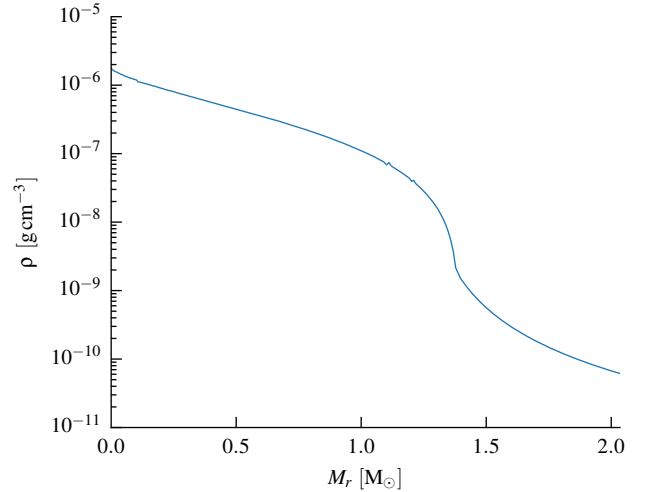
| Quantity | Value |
|------------------|-----------------------------------|
| M_{tot} | $1.39 M_{\odot}$ |
| M_{Ni} | $1.00 M_{\odot}$ |
| M_{Fe} | $0.10 M_{\odot}$ |
| $M_{\text{C/O}}$ | $0.18 M_{\odot}$ |
| M_{IME} | $0.10 M_{\odot}$ |
| E_{kin} | $1.44 \times 10^{51} \text{ erg}$ |

**Figure 1.** Illustration of the abundance structure of the ejecta model m100101. The mass fraction X of a number of important elements and isotopes is shown.

09dc-tail, mimicking the effects of ejecta–CSM interaction. The model was constructed to reflect the situation of a Chandrasekhar mass explosion, having produced $1.0 M_{\odot}$ nickel, interacting with a pure carbon-oxygen CSM with a mass of $M_{\text{CSM}} \approx 0.65 M_{\odot}$. Since hydrodynamic and radiation hydrodynamic effects have been neglected, the consequences of ejecta–CSM interaction are crudely taken into account by a global increase of the density (which is set up as an exponential profile).

Our numerical calculations are inspired by the 09dc-tail model, but we aim at a self-consistent treatment, in particular of the interaction phase and its consequences. For this purpose, we rely on the suite of explosion models produced by Woosley et al. (2007) to initiate the ejecta in our simulations. In these explosion calculations, the ejecta structure and evolution has been solved self-consistently in accordance with the energy released in the thermonuclear burning leading to a pre-defined ejecta composition. In particular, we rely on the model m100101 of the series which closely reflects the parameters adopted by Taubenberger et al. (2013). The main characteristics of this ejecta model are summarised in Table 1 and its detailed elemental composition is illustrated in Figure 1.

We embed the ejecta into a dense CSM of $M_{\text{CSM}} = 0.64 M_{\odot}$, again very similar to the choices of Taubenberger et al. (2013). This material is assumed to be free of hydrogen and helium but rich in carbon and oxygen and of uniform composition. The CSM composition can be

**Figure 2.** Density profile of the ejecta–CSM model which is used as the starting point for our STELLA simulations, $t_{\text{exp}} = 10^4$ s after explosion.

described by

$$X_i = \begin{cases} f_Z X_{i,\odot} & i = 7, i > 8 \\ (1 - f_Z X_{7,\odot} - f_Z \sum_{i>8} X_{i,\odot}) / 2 & i = 6, 8 \\ 0 & i < 6 \end{cases} \quad (1)$$

with X_i denoting the mass fraction of the element with proton number i . The scaling factor f_Z is a measure for the amount of non carbon-oxygen material in the CSM relative to solar abundances. We start our investigation with $f_Z = 1$, i.e. using solar abundances for all elements up to $Z = 28$, except for hydrogen, helium, lithium, beryllium, boron (which are all zero) and carbon and oxygen (which make up the remaining mass in equal parts). We further assume that the CSM is initially at rest and follows a power-law density profile, i.e.

$$\rho_{\text{CSM}} \propto r^{-p}. \quad (2)$$

with $p = 2$, extending up to an outer radius $R_{\text{CSM}} = 1.3 \times 10^{14} \text{ cm}$, which coincides with the outer boundary of the computational domain. The resulting density structure of the complete model is shown in Figure 2.

3.2 Numerical Method

To accurately track the shock-heating and compression processes together with the simultaneous transport of radiative energy generated in the ejecta–CSM interaction and produced by radioactivity, a radiation hydrodynamical treatment is required. For this purpose, we rely on the numerical code STELLA (Blinnikov & Bartunov 1993; Blinnikov et al. 1998, 2006). A number of design features render this code an ideal choice for studying interacting supernovae, in particular its fully implicit treatment of the radiation hydrodynamical problem and the Lagrangian description of fluid dynamics. These characteristics are particularly important when dealing with the strong forward and reverse shocks which are expected to form at the ejecta–CSM interface. A

Lagrangian treatment, in which the computational discretisation naturally adapts to the local fluid flow, is ideal for accurately tracking and resolving the large density contrasts in the vicinity of the shocks.

To address radiation hydrodynamical problems, it is often advantageous to rely on fully implicit treatments due to discrepancies between the characteristic flow and radiative time scales (see for example [Lowrie et al. 1999](#); [Sekora & Stone 2010](#), for a discussion of the radiation hydrodynamical coupling). This concern is particularly relevant for the type of problem investigated in this work. Due to the high kinetic energy of the ejecta material, intense heating is expected to occur at the shocks. The characteristic time scales of the resulting cooling processes may easily become much smaller than the hydrodynamic scales. This typically poses problems when relying on explicit time-stepping procedures¹ since all relevant time scales have to be resolved.

Given STELLA's advantages, it is ideally suited to study interacting supernovae and has been used for this purpose on numerous occasions (e.g. [Blinnikov & Sorokina 2010](#); [Baklanov et al. 2015](#); [Sorokina et al. 2016](#)). Since STELLA is a well-established technique, we only highlight some key aspects of the implemented physical processes and numerical techniques here. More details may be found in [Blinnikov & Bartunov \(1993\)](#); [Blinnikov et al. \(1998, 2006\)](#). STELLA operates on a one-dimensional, spherically symmetric, Lagrangian mesh and solves the full radiation hydrodynamical problem implicitly, including multi-group radiative transfer in the co-moving frame. The equations are discretised using finite differences for spatial and frequency derivatives, resulting in a large system of ordinary differential equations in time. This flavour of the method of lines (c.f. [Oran & Boris 1987](#)) is solved by using the multi-step predictor-corrector schemes of [Gear \(1971\)](#) and [Bryton et al. \(1972\)](#).

When calculating the radiation-matter coupling, STELLA takes contributions due to electron scattering, inverse bremsstrahlung, photoionization and interactions with atomic lines into account. For the last process, the expansion opacity treatment of [Friend & Castor \(1983\)](#); [Eastman & Pinto \(1993\)](#) is adopted (see details in [Blinnikov et al. 1998](#)). In addition to the multi-group radiative transfer treatment, a single-group γ -transport scheme is included to account for the energy deposition due to the main radioactive decay chain in SNe Ia, $^{56}\text{Ni} \rightarrow ^{56}\text{Co} \rightarrow ^{56}\text{Fe}$ ([Blinnikov et al. 2006](#)).

The radiative transfer treatment just detailed is less sophisticated than in dedicated pure radiative transfer and spectral synthesis approaches, such as ARTIS ([Kromer & Sim 2009](#)), CMFGEN ([Hillier & Miller 1998](#); [Hillier & Dessart 2012](#)), PHOENIX ([Hauschildt & Baron 2004](#)), SEDONA ([Kasen et al. 2006](#)) or SUPERNU ([Wollaeger et al. 2013](#); [Wollaeger & van Rossum 2014](#)). Moreover, the STELLA calculations are currently restricted to one-dimensional spherically symmetric setups. Both compromises are owed to STELLA's fully implicit design and its ambition to solve the fully coupled radiation hydrodynamical equations, properties which are crucial for the

type of problem investigated here (but see also discussion in Sections 5.2 and 5.4).

3.3 Numerical Setup

All results described in the following have been obtained in simulations with the same numerical parameters (exceptions are explicitly stated). The input model has been discretised on a Lagrangian mesh with 358 shells, with the ejecta model occupying the first half and with the remaining cells describing the CSM configuration. In addition to the spatial discretisation, the frequency space between 6.10×10^{13} Hz and 2.94×10^{18} Hz has been subdivided into 300 logarithmically spaced bins. This range corresponds to the wavelength regime 1.02 \AA and $4.91 \times 10^4 \text{ \AA}$. All simulations are started $t_{\text{exp}} = 10^4$ s after explosion (c.f. Section 3.1). An overview of all the calculations performed and presented in this work is provided in Table 2.

4 CALCULATIONS AND RESULTS

By following the radiation hydrodynamical evolution of the input model described in Section 3.1 with STELLA, we aim at exploring the consequences of thermonuclear explosions occurring within a dense and compact CSM (see sections 4.1 and 4.2). In addition, we examine whether the ensuing ejecta-CSM interaction may explain the peculiar properties of Super-Chandrasekhar objects by performing a detailed comparison with SN 2009dc in Section 4.3.

4.1 General Model Evolution

At the ejecta-CSM interface, fast moving ejecta material collides with the initially inert CSM. As a consequence, strong forward and reverse shocks emerge from the interface at the start of the calculations. The forward shock ploughs through the CSM and continuously sweeps up material while the reverse shock propagates into the ejecta in a Lagrangian sense, i.e. penetrating ever smaller mass shells². By this process the reverse shock continuously compresses, heats and decelerates the ejecta material as illustrated in Figure 3. Due to the compact configuration of the CSM, the forward shock quickly sweeps over the entire ambient material, after which the continuous conversion of kinetic into thermal energy subsides. This occurs at about $t \approx 1.2$ d, after which the model quickly readjusts and establishes a homologously expanding flow as illustrated in Figure 4. We note that, unless explicitly stated otherwise, we do not express time during the model evolution relative to the explosion point, but apply a crude ‘light travel correction’, accounting for the continuous expansion of the Lagrangian numerical grid. In particular, for a snapshot at t_{exp} after explosion, at which the outer edge of the computational domain is at r_{out} , this ‘observer time’ is given by

$$t = t_{\text{exp}} - \frac{r_{\text{out}}}{c}. \quad (3)$$

Here, the speed of light c appears.

¹ In the context of finite volume schemes, this is often referred to as the stiff source term regime (e.g. [LeVeque 2002](#)).

² Note that the radius of the reverse shock still continuously increases with time.

Table 2. Overview of the different ejecta-CSM configurations investigated and presented in this work. The number of radial shells N_{shells} , the total mass of the CSM M_{CSM} and its composition in terms of the parameter f_Z (see Equation 1) are provided. Also, the starting time of the calculation, t_{exp} , and the outer radius, R_{out} of the computational domain are indicated. The latter corresponds to the initial outer edge of the CSM envelope except for the pure ejecta model. Here, R_{out} denotes the radius of the outer edge of the ejecta.

| model name | N_{shells} | $M_{\text{CSM}} [M_{\odot}]$ | f_Z | $t_{\text{exp}} [\text{s}]$ | $R_{\text{out}} [\text{cm}]$ | notes |
|--------------------------|---------------------|------------------------------|-------|-----------------------------|------------------------------|---|
| m100101_nocsm | 179 | 0 | N/A | 10^4 | 2.53×10^{13} | bare ejecta model |
| m100101_csm_solar | 358 | 0.64 | 1 | 10^4 | 1.28×10^{14} | fiducial interaction model |
| m100101_csm_fZ2 | 358 | 0.64 | 2 | 10^4 | 1.28×10^{14} | |
| m100101_csm_fZ5 | 358 | 0.64 | 5 | 10^4 | 1.28×10^{14} | |
| m100101_csm_fZ20 | 358 | 0.64 | 20 | 10^4 | 1.28×10^{14} | best-fit model concerning light curve shape |
| m100101_csm_fZ100 | 358 | 0.64 | 100 | 10^4 | 1.28×10^{14} | |
| m100101_bigcsm_solar | 358 | 1.28 | 1 | 10^4 | 1.28×10^{14} | |
| m100101_csm_solar_1000 | 358 | 0.64 | 1 | 10^3 | 1.29×10^{14} | |
| m100101_csm_solar_100 | 358 | 0.64 | 1 | 10^2 | 1.31×10^{14} | |
| m100101_csm_solar_100_R5 | 358 | 0.64 | 1 | 10^2 | 5.21×10^{13} | |
| m100101_csm_solar_100_R2 | 358 | 0.64 | 1 | 10^2 | 2.59×10^{13} | |
| m100101_csm_solar_100_R1 | 358 | 0.64 | 1 | 10^2 | 1.29×10^{13} | |

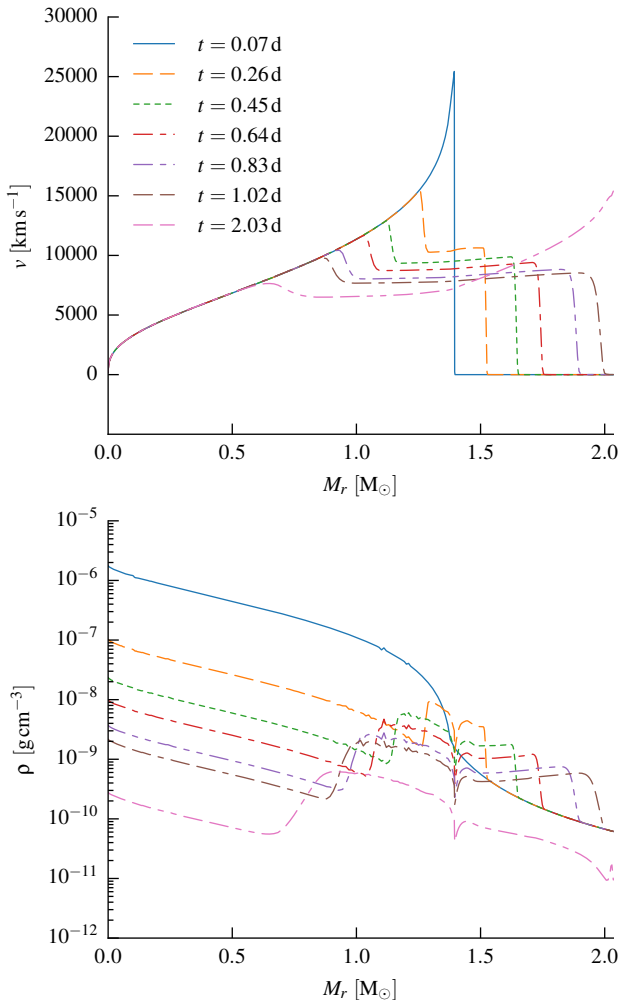


Figure 3. Velocity (upper panel) and density (lower panel) evolution of the interacting SN Ia model m100101_csm_solar. Different snapshots are shown. The reverse shock steadily propagates inwards in mass-space, compressing and decelerating the ejecta material. The same qualitative behaviour is observed in all other interaction calculations performed in this work as well.

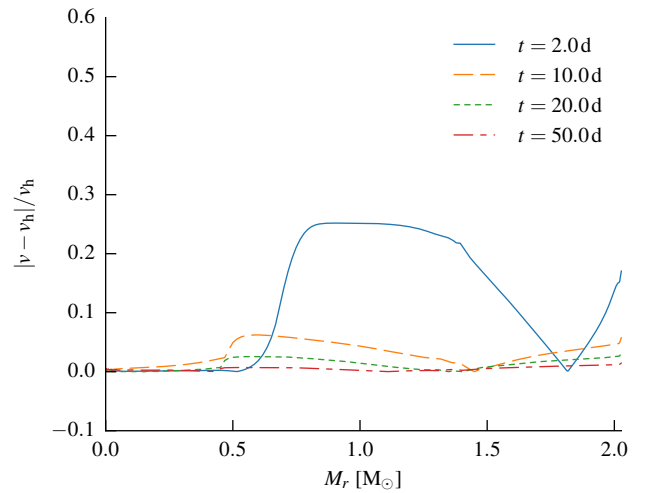


Figure 4. Relative deviation from homology in the ejecta-CSM interaction model m100101_csm_solar for a number of snapshots after the forward shock has swept up the entire CSM. Already at time $t = 10$ d, the largest deviations are less than ten per cent. Note that the time since explosion, t_{exp} , is used for the determination of the homologous expansion velocity $v_h = r/t_{\text{exp}}$.

4.2 Light Curve

During the ejecta-CSM interaction phase, very high temperatures are induced in the shock region, leading to intense emission of radiation from the shock front. Due to the high temperatures, the radiation is mostly emitted in the extreme ultraviolet and X-ray bands. This leads to an intense short-duration flash in this regime as seen in Figure 5. The light curves shown there are determined by applying cuts to the SED of the emergent radiation field as detailed in Table 3. Only a small fraction of the radiation in the high energy regime is reprocessed and shifted into the optical bands by interactions in the un-shocked material. This behaviour leads to a first bump in the *UBVRI* light curve as seen in Figure 5.

After the forward shock has reached the outer CSM edge, the shock heating ceases, the shocked material gradually cools and the nickel decay becomes the dominant process in shaping the light curve. Compared to a ‘bare’ ejecta

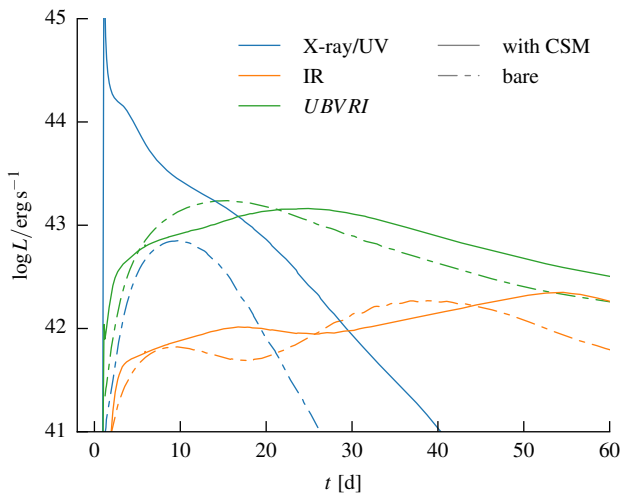


Figure 5. Comparison between the different broad-band light curves of the interacting SN Ia model (`m100101_csm_solar`, solid lines) and a corresponding calculation in which only the bare ejecta has been considered (`m100101_nocsm`, dashed lines). Note that the light curves have been determined by applying simple cuts to the SED (c.f. Table 3).

Table 3. Cuts in wavelength space which have been applied to determine the model light curves in the different regimes from the emergent SED in the *STELLA* calculations. In addition, the number of bins of the logarithmically spaced frequency grid (see Section 3.3), which discretize the different regimes, N_ν , are indicated.

| regime | λ_{\min} [Å] | λ_{\max} [Å] | N_ν |
|----------|----------------------|----------------------|---------|
| X-ray/UV | 1 | 3250 | 224 |
| UBVRI | 3250 | 8900 | 28 |
| IR | 8900 | 49000 | 48 |

calculation (`m100101_nocsm`), however, an increased trapping of γ and optical radiation is observed. This is caused on the one hand by the additional material which has been piled upon the ejecta and on the other hand by the density enhancement due to the shock compression. This leads to a longer rise time, a broadening of the peak and to a slower decline in the tail regime as highlighted by the comparison with the results of the ‘bare’ ejecta calculation `m100101_nocsm`, which are included in Figure 5. However, due to the small extent of the CSM configuration in our calculations, the ensuing ejecta–CSM interaction does not lead to a significant boost in the optical light curve around maximum.

4.3 Comparison with SN 2009dc

As outlined above in the generic description of the model evolution, the ejecta–CSM interaction induces a number of features which qualitatively match some of the defining properties of the class of Super-Chandrasekhar objects. For a more detailed assessment of the validity of the proposed scenario, we perform in the following sections a detailed quantitative comparison between the model properties and the observed data of the prototype of the class, SN 2009dc.

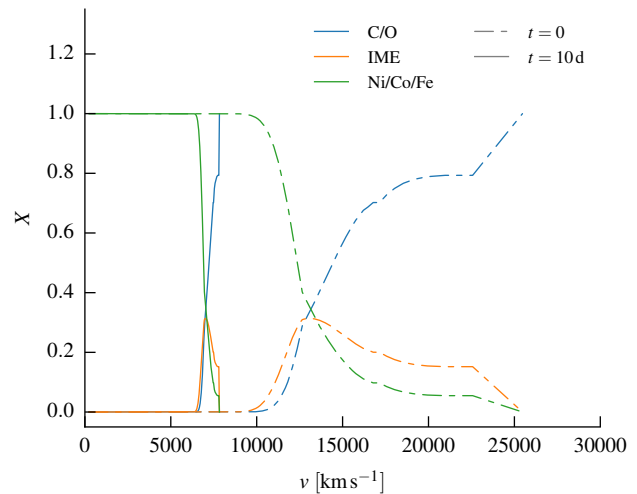


Figure 6. Comparison of the initial distribution of a number of selected elements in the ejecta material to that after the main ejecta–CSM interaction phase in `m100101_csm_solar`. In particular, the situation at $t = 10$ d is shown. By that time, the reverse shock has efficiently decelerated most of the ejecta material.

4.3.1 Line Velocities

Among the striking properties of SN 2009dc are its peculiar line velocities, which are consistently lower than in normal SNe Ia (e.g. Taubenberger et al. 2011). In the investigated model, the strong reverse shock quickly and efficiently decelerates the ejecta material. This leads to an elemental distribution in velocity space which is significantly compressed compared to that of a typical SN Ia. Figure 6 illustrates this behaviour in `m100101_csm_solar` by comparing the initial stratification of the ejecta material (representative of the situation in a typical SN Ia) with the situation after the interaction phase, roughly at the time when homology is nearly re-established. Already at this early time, i.e. $t = 10$ d, all intermediate-mass elements (IME) are confined to a very small low-velocity region, ranging from about 6000 km s^{-1} to 8000 km s^{-1} . This distribution is compatible with the line velocities determined for SN 2009dc: in particular Taubenberger et al. (2013) established that the Si II $\lambda 6355$ line velocity lies between 6000 km s^{-1} and 9000 km s^{-1} .

One should emphasise that this consideration has solely been based on the elemental distribution in velocity space, without taking the details of the line formation process into account. Ideally, the line velocities would be validated by comparing synthetic with observed spectra. However, the SEDs provided by *STELLA* are much too coarse for this purpose. Nevertheless, a necessary condition for the appearance of certain line velocities in the observed spectral features is the location of the corresponding elements in the appropriate velocity regime.

4.3.2 UBVRI Light Curve

As highlighted in Section 4.2 and illustrated in Figure 5, the interaction between ejecta and CSM leads to a slower rise of the *UBVRI* light curve, a broadening of its overall shape and a slower decline – all properties which have been

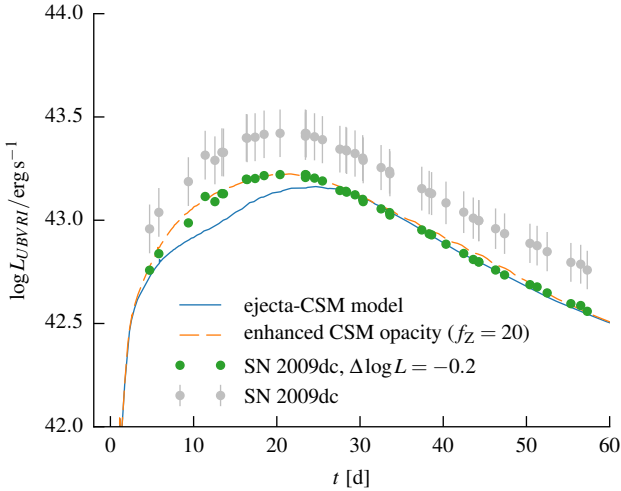


Figure 7. Comparison between the synthetic *UBVRI* light curve of the interacting model (`m100101_csm_solar`, solid blue line) and the corresponding observed luminosities for SN 2009dc (grey symbols). The displayed uncertainty ranges are due to distance and reddening. To highlight the good match between the synthetic light curve shape and the observed evolution, a comparison with the observed data shifted by $\Delta \log L / \text{erg s}^{-1} = -0.2$ (green symbols) is included as well. An even better match to the light curve shape is achieved when enhancing the reprocessing efficiency in the CSM (by artificially boosting the content of non-carbon-oxygen material in the CSM, see Section 4.3.3). The synthetic *UBVRI* light curve of one such calculation, with $f_Z = 20$, (see Equation 1) is included (`m100101_csm_fZ20`, dashed orange line)

observed in SN 2009dc. However, when directly comparing the synthetic *UBVRI* light curve with the observed data of SN 2009dc, as done in Figure 7, the missing overall luminosity boost becomes apparent. In particular, the STELLA model light curve is during all phases too dim by about 0.2 dex. This discrepancy goes beyond the uncertainties set by the distance determination and adopted reddening prescription for SN 2009dc (see Taubenberger et al. 2011). Despite this mismatch on absolute scales, the interaction model reproduces the observed light curve shape remarkably well. This is illustrated in the comparison shown in Figure 7, in which a global, artificial shift of 0.2 dex has been applied to the SN 2009dc observations. This is comparable to the assumption made by Kamiya et al. (2012) that there be no host galaxy extinction³.

4.3.3 Addressing the Peak

The largest discrepancy in the light curve shape between model and observations manifests around the peak (see Figure 7). During this phase, the model exhibits two pronounced plateaus. The initial steep rise represents the optical afterglow of the interaction phase which is superimposed on the normal typical light curve evolution due to radioactive heating. As a consequence of the shock compression,

the radioactive signal is delayed. In the peak region, the synthetic light curve is also lacking more luminosity than in the other regimes.

The ejecta-CSM interaction nevertheless generates a substantial amount of radiative energy. However, due to the high shock temperatures this energy is mostly released in the X-ray and far UV regime. Only a small fraction is reprocessed by interacting in the CSM, thus producing the optical afterglow seen as the first plateau in the light curve.

This leads to the conclusion that a luminosity boost may still be achieved within the proposed interaction scenario, provided that the re-processing efficiency can be enhanced. To demonstrate this, we artificially boost the opacity in the CSM. A simple way to achieve this within the STELLA framework to increase the amount of non-carbon-oxygen material. For simplicity, we just scale the solar abundances for all elements heavier than $Z = 8$ (including nitrogen) and set the remainder to carbon and oxygen in equal parts. Thus, we use a scaling parameter f_Z different from one in Equation (1). Figure 8 illustrates the consequences of boosting the non-carbon-oxygen material according to the prescription (1). The increase in opacity when using higher metal contents in the CSM is shown in terms of the corresponding absorption-mean (c.f. Mihalas & Mihalas 1984, §82)

$$\kappa_J = \frac{\int d\nu \kappa_\nu J_\nu}{\int d\nu J_\nu}, \quad (4)$$

involving a frequency integration of the absorption opacity κ_ν , weighted by the mean intensity J_ν . As the opacity and thus the reprocessing efficiency in the CSM increases, the *UBVRI* luminosity in the peak region is steadily boosted. Figure 7 also compares the synthetic light curve of the $f_Z = 20$ calculation, `m100101_csm_fZ20`, with the SN 2009dc observations (still shifted by 0.2 dex), now showing a perfect match in the light curve shape.

We emphasize that this exploration only serves to illustrate the general consequences of having a high reprocessing efficiency for energetic radiation in the CSM. This significantly improves the observable optical light curve of the interacting model. We stress, however, that these results should not be interpreted as indications for the presence of a particular type of CSM with a high amount of non-carbon-oxygen material. In fact, Childress et al. (2011) and Khan et al. (2011) suggest low-metallicity environments for Super-Chandrasekhar events. Instead, we consider the CSM composition change a simple realisation of enhancing the opacity in the STELLA framework and as a potential representation of interaction processes which are not fully incorporated in the simplified radiative transfer treatment adopted in STELLA. One such shortcoming is the small number of atomic line transitions taken into account. A more detailed discussion of this point will follow in Section 5.4.

4.3.4 Addressing the Tail

The experiments with an enhanced opacity in the CSM described in the previous section nicely lead to a luminosity boost around the peak. However, the post-maximum decline and the tail of the light curve are largely unaffected by these changes in the CSM composition (see top panel in Figure 8). But also during these phases, the synthetic light curves of

³ Note that the complete absence of any host extinction is ruled out by the detection of interstellar sodium lines at the redshift of the host of SN 2009dc (e.g. Taubenberger et al. 2011).

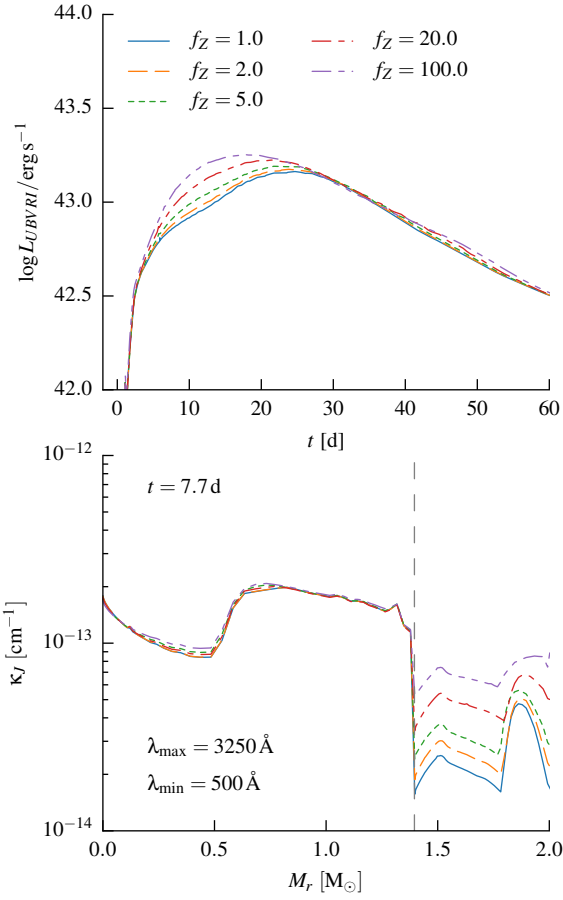


Figure 8. Consequences of increasing the opacity in the CSM by changing its composition according to Equation (1). In particular, the models `m100101_csm_solar`, `m100101_csm_fZ2`, `m100101_csm_fZ5`, `m100101_csm_fZ20` and `m100101_csm_fZ100` are shown. The composition change leads to a stronger redistribution of high energy radiation generated during the ejecta–CSM interaction into the optical *UBVRI* bands around peak (upper panel). In the bottom panel, the increase in opacity when changing f_Z is illustrated in terms of the absorption-mean κ_J (see Equation 4), evaluated in the range $500 \text{ \AA} \leq c/\nu \leq 3250 \text{ \AA}$.

the interaction models are too dim and would require a boost of 0.2 dex to be compatible with the observations.

At first glance, this discrepancy in the light curve tail is unexpected given that the ejecta–CSM interaction models have been constructed to reflect the global properties of the toy model `09dc-tail` presented by Taubenberger et al. (2013), as detailed in Section 3.1. The `09dc-tail` toy model has been specifically designed to reproduce the tail light curve of SN 2009dc both in shape and in absolute scale. However, simplistic assumptions about the effects of ejecta–CSM interaction have been adopted in the toy model (due to the lack of a self-consistent radiation hydrodynamical treatments). More specifically, the density profile has been globally up-scaled to approximately reflect the compression by the reverse shock. This idealistic situation is not observed

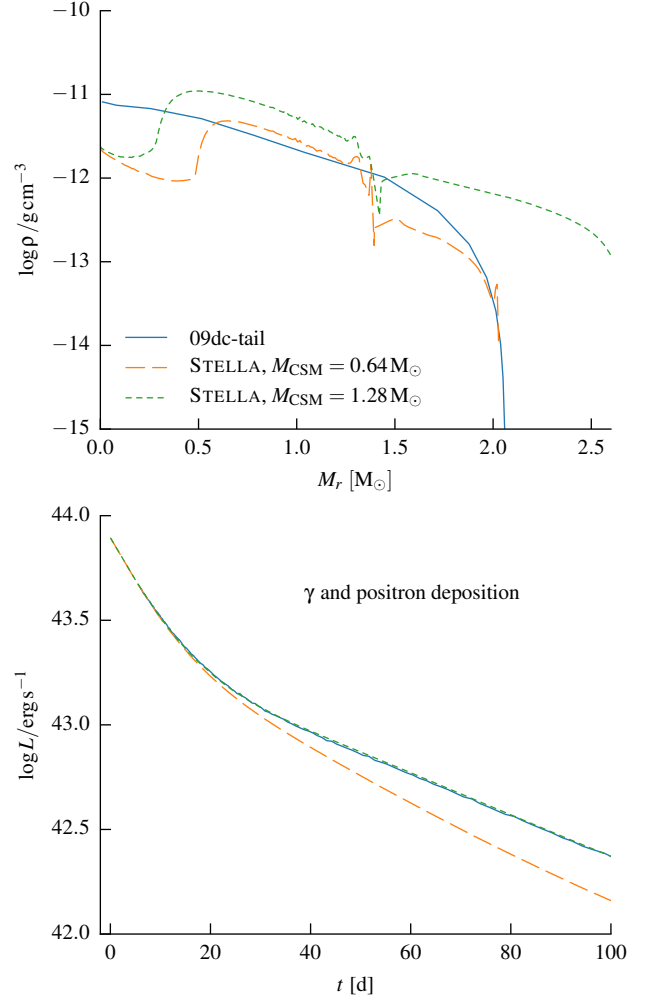


Figure 9. Comparison between the density profiles of the STELLA interaction model (with $M_{\text{CSM}} = 0.64 M_{\odot}$, `m100101_csm_solar`) and the toy model `09dc-tail` by Taubenberger et al. (2013) at $t = 10$ d (upper panel). The reverse shock has stopped its propagation after reaching the mass shell $M_r = 0.5 M_{\odot}$. During the following evolution of the model, the density discontinuity is simply advected by the expanding flow. As a consequence of the differences in central densities, γ -ray trapping is less efficient in STELLA than in the ARTIS (Kromer & Sim 2009) radiative transfer calculations used by Taubenberger et al. (2013). The γ -deposition (lower panel) between the model differs by a factor of 1.5, exactly the same value by which the *UBVRI* light curves are different. For comparison, results of a STELLA calculation with higher CSM mass, $M_{\text{CSM}} = 1.28 M_{\odot}$ (`m100101_bigcsm_solar`), and thus a stronger reverse shock are also included.

in our models, in which the shock compression is treated self-consistently. As illustrated in Figure 9, the compression of the density profile only reaches down to the mass shell $M_r \approx 0.5 M_{\odot}$. The ongoing compression of the material lying above this shell has exhausted the energy of the reverse shock. The density discontinuity is simply advected by the expanding flow and the inner core region remains un-compressed. As a consequence, the density within a significant fraction of the nickel core is much lower than under the idealised assumptions of the toy-model. This leads to a significant difference in the γ -trapping efficiency, which

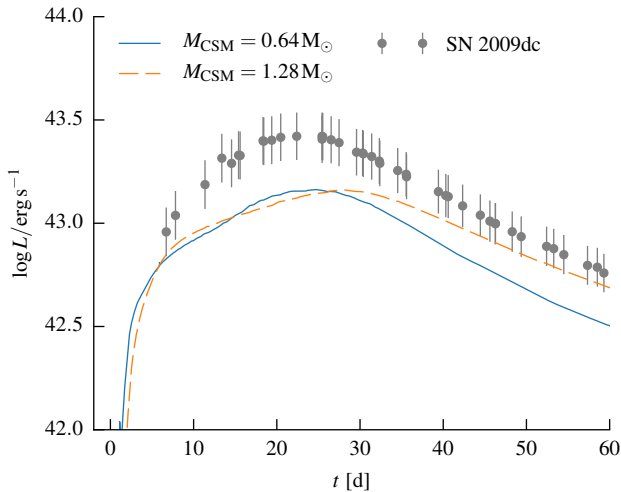


Figure 10. Comparison between the synthetic *UBVRI* light curve of the high-CSM-mass STELLA model `m100101_bigcsm_solar` and the (original) SN 2009dc observations. Due to the higher compression of the ejecta, the light curve tail now better matches the observations. However, the elemental distribution in velocity space is now incompatible with the line velocity observations of SN 2009dc (see Figure 11). As a comparison, the light curve of the standard STELLA interaction model, `m100101_csm_solar`, is included as well.

mainly determines the light curve evolution past maximum. Due to the lower column density in the STELLA model, γ -radiation can escape more easily and the γ -deposition within the ejecta is lower by roughly the same amount as in the *UBVRI* light curve (see lower panel of Figure 9).

These findings seem to indicate that a stronger compression of the nickel zone is required to boost the tail light curve. This suspicion is confirmed by a STELLA test calculation, `m100101_bigcsm_solar`, in which a higher CSM mass is used ($M_{\text{CSM}} = 1.28 M_{\odot}$). A stronger reverse shock is generated in this calculation, which penetrates deeper layers, down to $M_r \approx 0.2 M_{\odot}$ and thus leads to an overall stronger compression (see Figure 9). As expected, γ -trapping is enhanced, leading to a slower decline of the light curve during the tail phase as illustrated in Figure 10. However, the higher compression is achieved by a stronger deceleration of the ejecta material, inducing an elemental distribution which seems to be inconsistent with observations for SN 2009dc (see Figure 11). These findings put a strain on the otherwise quite successful interaction model. The strong trapping during the tail phase seems to require an intense compression of the ejecta, only achievable by a strong reverse shock. This inevitably leads to a strong deceleration of the ejecta material, which seems to be stronger than observed.

5 DISCUSSION

By performing a series of STELLA calculations, we have identified a number of generic consequences of fairly normal SN Ia exploding within a dense compact carbon and oxygen rich envelope. Having presented these findings in the previous sections, we briefly discuss a progenitor scenario which may provide a CSM environment as investigated here. We

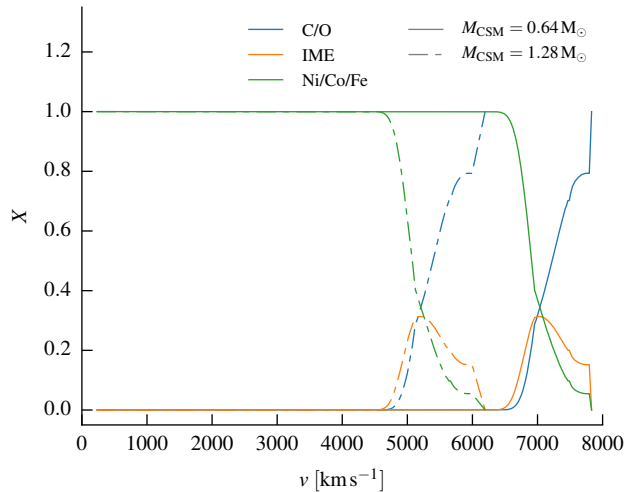


Figure 11. Final (at $t = 10$ d after explosion) elemental distribution in the normal and high-CSM-mass STELLA interaction model, `m100101_csm_solar` and `m100101_bigcsm_solar` respectively. The more powerful reverse shock in the latter one leads to a much stronger deceleration of the ejecta material.

also briefly re-examine our findings in light of some limitations of our approach and finally assess a possible link between interacting SNe Ia and Super-Chandrasekhar explosions.

5.1 CSM Origin

Within the context of SNe Ia, the double degenerate mechanism is the most plausible scenario to provide a CSM configuration and composition as investigated in this work. In contrast to the recent advancement and success of the violent merger scenario, involving a prompt explosion (e.g. Pakmor et al. 2010, 2012; Moll et al. 2014), we consider the classical mechanism (Webbink 1984), in which the secondary WD is completely disrupted before a thermonuclear runaway can set in, as the most probable candidate. Yoon et al. (2007) showed that in this scenario, the subsequent accretion of the disrupted secondary leads to the formation of a hot nearly-spherical hydrostatic atmosphere and an extended thick accretion disk. This material would qualitatively qualify for the carbon and oxygen rich CSM investigated in this study. However, we caution that it is still a matter of ongoing debate whether such a ‘slow merger’ would eventually lead to a thermonuclear explosion and thus potentially to an SN Ia event or whether an accretion induced collapse would be triggered (see e.g. Yoon et al. 2007; Shen et al. 2012). Nevertheless, this scenario has been investigated previously, e.g. by Raskin et al. (2014). Such explosions are often linked to ‘tamped detonations’, studied extensively by Khokhlov et al. (1993); Hoefflich & Khokhlov (1996), and have been suggested as models for Super-Chandrasekhar SNe Ia (e.g. Scalzo et al. 2014; Raskin et al. 2014).

5.2 Geometry

All calculations presented here have been performed assuming perfect spherical symmetry. This assumption naturally

not only applies to the geometry of the supernova ejecta but extends also to the CSM configuration. These simplifications, which are owed to STELLA's restriction to one-dimensional spherically symmetric computational meshes, are acceptable for wind-like CSM scenarios. However, as detailed above, the specific CSM composition considered here suggests an association with the double-degenerate scenario, in particular with the 'slow-merger' model.

Even though the material in the immediate vicinity of the primary WD and thus the explosion site is expected to establish an extended, nearly spherical envelope, a prominent thick disk component should form as well (Yoon et al. 2007). Consequently, strong deviations from spherical symmetry are expected at least in this part of the circumstellar environment. Ejecta-CSM interaction occurring in this configuration may lead to different signatures along different lines of sight. The importance of varying column optical depth along different lines of sight in the context of the most luminous SNe Ia has already been highlighted by Hillebrandt et al. (2007) and was seen, for example, in the tamped detonation calculations by Raskin et al. (2014). In the context of Super-Chandrasekhar events, such line-of-sight effects may explain part of the diversity of the class of objects. In addition, due to the anisotropic CSM distribution, the reverse shock may have variable strength in different regions, leading to various degrees of deceleration of the ejecta material. Again, this may help resolve the difficulties reported in the previous section concerning the tail phase, namely achieving a sufficiently strong γ -trapping without decelerating the ejecta material too drastically. However, we emphasize that the exact consequences of these geometrical effects are hard to predict. In fact, they cannot be adequately captured with our simple one-dimensional approach. Instead a fully-fledged multidimensional radiation hydrodynamical treatment, capable of accounting for a multitude of line interactions would be required. In this respect, Monte Carlo-based approaches, such as Noebauer et al. (2012); Roth & Kasen (2015); Harries (2015), hold some promise, but the time scales constraint discussed in Section 3.2 may prove problematic. Moreover, many of the cited methods have not yet been generalised to multidimensional geometries or are designed for applications that are quite different from interacting supernovae. In light of these considerations of geometrical limitations, our study should be viewed as a first exploration, investigating the overall effect of ejecta-CSM interaction and its general plausibility as a model for Super-Chandrasekhar objects.

5.3 Compactness

In the current investigation, the STELLA calculations have been started at $t_{\text{exp}} = 1 \times 10^4$ s after explosion for reasons of computational convenience. Thus, before interacting with the CSM, the ejecta have already expanded significantly leading to a substantial drop in density. Within the 'slow-merger' picture, however, the ejecta-CSM interaction would be expected to set in at earlier times, thus implying a more compact configuration with both the ejecta and the CSM at higher densities (c.f. Yoon et al. 2007).

We briefly investigate the consequences of ejecta-CSM interaction occurring in denser and more compact environments and explore specifically whether an increase in the

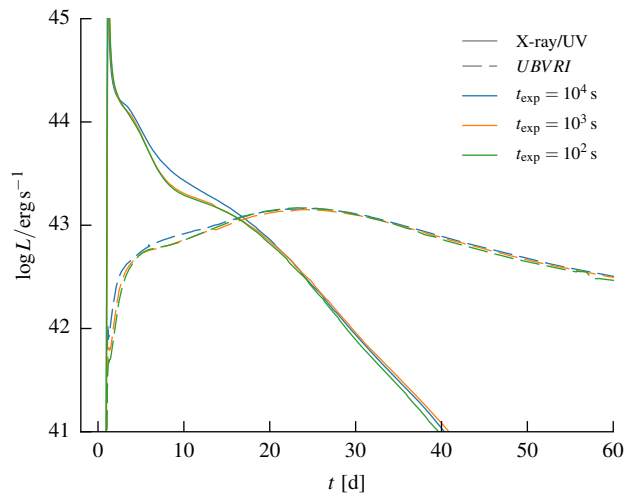


Figure 12. X-ray/UV and *UBVRI* light curves for the calculations `m100101_csm_solar`, `m100101_csm_solar_1000` and `m100101_csm_solar_100`. In this series, the time at which the STELLA calculations are started is reduced from 10^4 to 10^3 and 10^2 s, resulting in increasingly more compact and dense ejecta. The extent of the CSM envelope remains unchanged.

compactness may improve some of the current shortcomings of the fiducial model (`m100101_csm_solar`). First, the effects of reducing the time since explosion are explored. This change is later combined with an increase in the compactness of the CSM envelope. During the entire exploration, the total CSM mass remains unchanged.

Relying on the homologous expansion laws, the reduction of the time since explosion leads to a density increase in the ejecta according to $\rho(t) = \rho(t_0)(t_0/t)^3$. Here, t_0 denotes an arbitrary reference time. This boost of the ejecta density has only small effects on the amount of energy generated in the ejecta-CSM interaction and only induces insignificant changes in the X-ray/UV and *UBVRI* light curves. Figure 12 illustrates this behaviour in terms of the emergent *UBVRI* light curves for the calculations `m100101_csm_solar`, `m100101_csm_solar_1000`, `m100101_csm_solar_100` which were started at 10^4 , 10^3 and 10^2 s after explosion, respectively. Due to the changing ratio of ρ_{ejecta} and ρ_{CSM} , the deceleration of the ejecta material induced by the reverse shock decreases slightly in this series as shown in Figure 13.

Based on the model `m100101_csm_solar_100` with $t_{\text{exp}} = 10^2$ s we complete the exploration of more compact configurations by successively reducing the extent of the CSM envelope while keeping the enclosed mass constant. In this process, the CSM density is boosted. Following the model evolution with STELLA reveals that still large amounts of energy are released during the ejecta-CSM interaction. However, the interaction signature becomes successively weaker, particularly in the X-ray/UV regime but also in the *UBVRI* light curve, as shown in Figure 14. During the early evolution, the transition between the optically thick and the optically thin regime occurs deep inside the CSM envelope in the fiducial model `m100101_csm_solar`. By increasing the CSM density and reducing the outer CSM radius, this transition region is pushed closer to the surface of

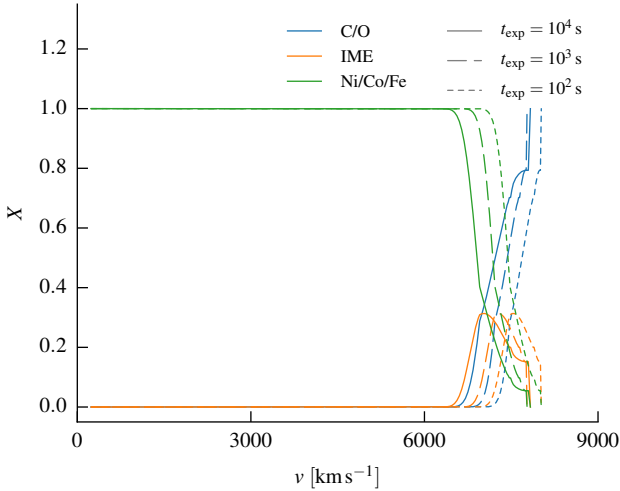


Figure 13. Elemental distribution at $t = 10$ d for the model series shown in Figure 12. The decelerating effect of the reverse shock becomes slightly weaker as the time since explosion decreases and thus the ejecta density increases.

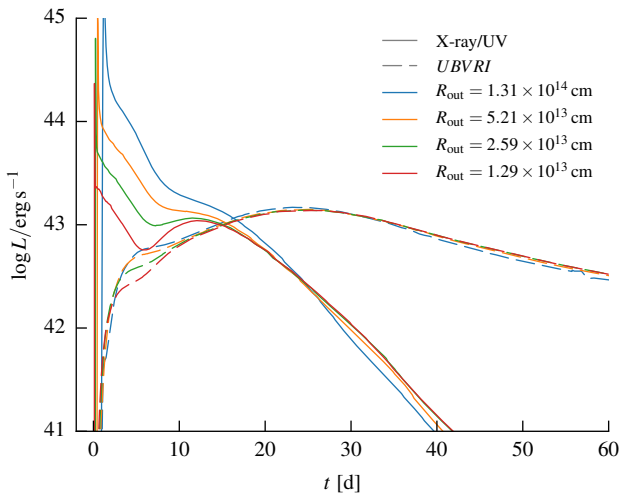


Figure 14. X-ray/UV and *UBVR* light curves for increasingly more compact ejecta-CSM configurations. In particular, the results of the calculations `m100101_csm_solar_100`, `m100101_csm_solar_100_R5`, `m100101_csm_solar_100_R2` and `m100101_csm_solar_100_R1` are shown. The decreasing release of interaction radiation is a consequence of the reduced size of the emitting system.

the CSM envelope. As a consequence, the radiation generated in the ejecta-CSM interaction breaks out of the system at smaller radii and less total energy is overall emitted.

This exploration demonstrates that within the simplified one-dimensional treatment and with the global parameters adopted here, a simple increase of the compactness of the ejecta-CSM configuration does not lead to an increase in the emitted radiation energy. However, this exploration should not be interpreted as a detailed investigation of the plausibility of the ‘slow-merger’ model in the context of interacting SNe Ia, most notably for the inadequate treatment

of its complex geometrical properties (c.f. Section 5.2) and due to the limited exploration of the involved parameters.

5.4 CSM Composition and Line List

It has already been highlighted at the outset (see Section 3.2), that STELLA sacrifices some details in the radiative transfer treatment in favour of a fully coupled radiation hydrodynamical solution strategy. With respect to modelling SNe Ia, the comparably small number of atomic line transitions included in the opacity calculation is a significant limitation. In a typical STELLA calculation, as presented here, $\approx 1.5 \times 10^5$ line transitions are taken into account. In contrast, dedicated pure radiative transfer simulations of SN Ia ejecta, for example performed with ARTIS (Kromer & Sim 2009), use up to millions of line transitions to accurately follow radiative transfer and the frequency redistribution occurring within SN Ia ejecta.

As a consequence of relying on the small line list of STELLA, an important contribution to the overall opacity within the model may be missed. The omitted processes may provide some of the necessary reprocessing of energetic radiation produced in the ejecta-CSM interaction into the optical bands. The exploratory test calculations performed with varying CSM compositions should be viewed in this light. By enhancing the content of non-carbon-oxygen material in the CSM, we boost the bound-bound opacity contribution and thus very crudely approximate the effect of using a more complete line list. We note that by using the prescription, we also enhance the bound-free contribution to the total opacity and may influence the overall plasma state in the CSM.

Nevertheless, using high amounts of non-carbon-oxygen material in the CSM qualitatively seems to be a valid representation of a larger line list. This statement is supported by test calculations performed with an experimental version of STELLA (Sorokina & Blinnikov 2016). With this variant of the code (referred to as STELLA-STAT in this work), a large number of atomic line transitions may be efficiently treated using a statistical approach. Repeating the simulation of the standard setup of the interaction model with a $f_Z = 1$ CSM composition and 26 million lines, taken from Kurucz (1993), shows that the optical luminosity stemming from the ejecta-CSM interaction around peak is boosted compared to the results obtained with the standard STELLA version and 155000 lines (see Figure 15). However, we repeat that the STELLA-STAT version is still under active development and not yet fully tested on different SN types.

From the exploratory test presented in Section 4.3.3 and the preliminary calculations performed with STELLA-STAT, we conclude that some of the discrepancies we see in the fiducial calculation with a $f_Z = 1$ CSM composition, `m100101_csm_solar`, may actually be attributed to the use of an incomplete line list and consequently to simplifications adopted in the radiative transfer treatment of STELLA. However, the few calculations performed with STELLA-STAT, are not sufficient to confidently assess whether these effects alone may fully account for the gap between model and SN 2009dc observations seen in Section 4.3.

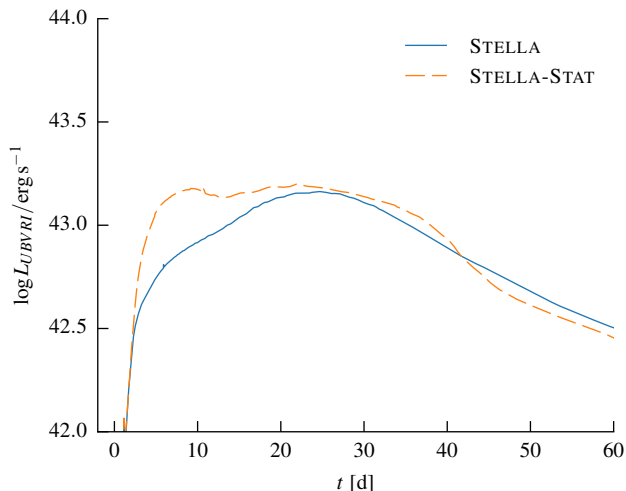


Figure 15. Comparison between the *UBVRI* light curve of the interaction model `m100101_csm_solar`, calculated with STELLA (155000 lines) and STELLA-STAT (26 million lines). The result from the latter clearly shows the importance of the line opacity for reprocessing the energetic radiation into the optical bands and thus qualitatively supports our tests with enhanced CSM opacities presented in Section 4.3.3.

5.5 Super-Chandrasekhar SNe from SNe Ia within dense Carbon-Oxygen Envelopes?

As the detailed comparison with SN 2009dc demonstrated (see Section 4.3), the proposed interaction scenario is able to explain a number of characteristic features of such Super-Chandrasekhar SNe Ia. The decelerating effect exerted onto the ejecta material by the reverse shock provides a natural explanation for the low line velocities observed in some Super-Chandrasekhar objects. In particular, the final elemental composition of the ejecta material observed in the STELLA simulations is compatible with the low line velocities measured for SN 2009dc. In addition, many properties of the optical light curve, such as a long rise and a slow decline, can be attributed to the density enhancement following the shock compression in the ejecta–CSM interaction. Specifically with respect to SN 2009dc, the light curve shape was nearly perfectly reproduced in the STELLA calculations. Finally, the composition of the CSM and the fact that it is quickly swept up by the ejecta, provides a natural explanation for the absence of any tell-tale interaction signatures in the observational data, such as narrow or intermediate-width hydrogen emission lines. Also, the high carbon content in the CSM could explain the strong and persistent carbon lines seen in many Super-Chandrasekhar SNe and facilitate dust formation which is suggested to occur in a number of these objects.

Despite the many successes of the interaction scenario, achieving a significant boost in the optical peak luminosity during the radiation hydrodynamical calculations proves challenging. The explorations performed in this work suggest that the reprocessing efficiency of highly energetic radiation is key for this. As demonstrated in Section 5.3, however, simply increasing the compactness of the ejecta–CSM configuration does not help. Instead, the associated column optical depth associated with the reprocessing effi-

ciency may for example be increased by higher CSM opacities. As detailed in Section 5.4, shortcomings of the radiative transfer treatment in STELLA could be partly responsible for too low a reprocessing efficiency in the current calculations. Also, line-of-sight effects, which are expected to occur when realistic geometries are considered (c.f. Section 5.2), may help in achieving a boost. Irrespective of these considerations, a number of Super-Chandrasekhar objects are less luminous than SN 2009dc, for example SN 2006gy or SN 2012dh. Their optical light curve peaks may already be reproduced by models presented here, independently of the consequences of omitted radiative transfer effects and geometrical influences.

In summary, given the many successes of the current interaction scenario with respect to reproducing properties of SN 2009dc, we consider it a promising candidate for explaining Super-Chandrasekhar SNe Ia. Additional explorations, which sample a wider parameter range, undertake detailed spectral synthesis calculations and address the inherent multidimensional geometry, are recommended to further support this claim.

6 SUMMARY AND CONCLUSIONS

In this work, we have investigated the consequences of SNe Ia being surrounded by a thick carbon-oxygen rich CSM envelope. Our main interest rested on studying the effect of the ensuing ejecta–CSM interaction on the ejecta evolution and on the emergent light curve. Here, we focussed on a particular realisation of this scenario, which has previously (c.f. Taubenberger et al. 2013) been identified as a promising candidate for the explanation of Super-Chandrasekhar SNe Ia, in particular for SN 2009dc.

We followed the evolution of the considered model using the radiation hydrodynamical code STELLA (Blinnikov & Bartunov 1993; Blinnikov et al. 1998, 2006). At the ejecta–CSM interface, a strong forward and reverse shock form, sweeping up the CSM and compressing the ejecta material, respectively. Due to the shock heating processes, a substantial amount of energy is injected into the radiation field. However, this occurs mostly in the X-ray and UV regime and only part of it is shifted into the optical *UBVRI* bands due to reprocessing in the CSM. As a consequence, no significant boost in the maximum *UBVRI* luminosity is observed compared to a corresponding ‘bare’ SN Ia explosion. However, we find that the ejecta–CSM interaction leads to a longer rise and a significant broadening of the light curve. Past maximum, a slower decline of the optical light curve is observed due to the increased γ -trapping induced by the compression of the ejecta material by the reverse shock. Apart from the density increase, the ejecta material has also been significantly decelerated, leading to an extended velocity plateau in mass space.

Despite the missing luminosity boost in the fiducial model, we find that an increase in the light output in the optical regime may still be achieved if the reprocessing efficiency in the CSM is enhanced. Not observing this in the current calculations may simply be a consequence of simplifications adopted in the radiative transfer scheme implemented in the standard version of STELLA. In particular, us-

ing a realistic near-complete line list significantly increases the opacity and the reprocessing efficiency. We performed simple test calculations with an enhanced CSM opacity and by carrying out calculations with an experimental STELLA version, capable of treating millions of atomic line transitions, supporting these statements. During the light curve decline phase, the increased γ -trapping is a direct consequence of the compression due to the reverse shock. Thus, its strength regulates the optical luminosity during these phases and an additional boost may consequently be achieved here, if the ejecta is, for example, embedded into a more massive CSM envelope.

In addition to these generic findings, the interaction scenario successfully reproduces a number of characteristic features of Super-Chandrasekhar SNe Ia, despite the difficulty to produce a significant luminosity boost in the optical light curve. When comparing to the prototype of this class, SN 2009dc, we find that the shape of the observed optical *UBVRI* light curve is almost perfectly matched. In particular, the long rise time, the broad maximum and the delayed decline due to increased γ -trapping is well reproduced. Moreover, the deceleration of the ejecta material due to the reverse shock provides a natural explanation for the low line velocities observed in SN 2009dc. The velocity distribution of the different elements found in the model is compatible with these observations. However, to establish a directly link, detailed spectral synthesis would have to be performed, a task which cannot be easily carried out with STELLA. Despite these successes, the defining characteristic feature of SN 2009dc, namely the high light output is not fully reproduced in the numerical calculations. However, as pointed out already above, limitations of the radiative transfer treatment in STELLA may be partly responsible for that.

Next to the compromises in the radiative transfer treatment, the restriction to spherically symmetric configurations is a shortcoming of the current study. In particular, if double degenerate scenarios are considered as the possible origin of the CSM material, deviations from spherical symmetry may play an important role. The exact consequences of these are difficult to predict, but line-of-sight effects seem plausible. To some extent, these could provide a natural explanation for some of the diversity seen in Super-Chandrasekhar objects.

In summary, despite some shortcomings of our current study, the initial investigation of SNe Ia interacting with a dense carbon-oxygen rich envelope shows that this scenario may provide a viable explanation for Super-Chandrasekhar objects. To further investigate this possibility and to better quantify the generic consequences of ejecta-CSM interaction, we aim to continue our study of this scenario in the future, specifically focussing on three points. Firstly, a better sampling of the possible parameter space, both in terms of the ejecta and the CSM properties, should be performed and thus different configurations of the interaction scenario investigated. In addition, we aim to map results from STELLA simulations into dedicated radiative transfer approaches, such as ARTIS (Kromer & Sim 2009) and TARDIS (Kerzendorf & Sim 2014), once homology is approximately retained. This way, detailed colour light curves may be determined and the spectral appearance of the interacting models predicted. In parallel, it should be explored how alternative radiation hydrodynamical methods, such as MCRH

(Noebauer et al. 2012, 2015), may be applied to the interacting SNe Ia problem, with the goal of eventually overcoming the current limitation to one-dimensional geometries. These steps will help establishing whether super-luminous SNe Ia are interaction-powered and whether and to which extent ejecta-CSM interaction is relevant for other SNe Ia.

ACKNOWLEDGEMENTS

The authors would like to thank M. Kromer, R. Pakmor and S. Sim for stimulating and fruitful discussions. The authors also thank the anonymous reviewer for valuable comments. This work has been supported by the Transregional Collaborative Research Center TRR33 ‘The Dark Universe’ of the Deutsche Forschungsgemeinschaft and by the Cluster of Excellence ‘Origin and Structure of the Universe’ at Munich Technical University. The work of SB (development of the code STELLA) has been supported by a grant of the Russian Science Foundation 14-12-00203, the work of ES (statistical approach for opacity calculation) has been supported by a grant of the Russian Science Foundation 16-12-10519.

REFERENCES

- Baklanov P. V., Sorokina E. I., Blinnikov S. I., 2015, *Astronomy Letters*, **41**, 95
- Barkat Z., Rakavy G., Sack N., 1967, *Phys. Rev. Lett.*, **18**, 379
- Blinnikov S. I., Bartunov O. S., 1993, *A&A*, **273**, 106
- Blinnikov S. I., Sorokina E. I., 2010, preprint, ([arXiv:1009.4353](https://arxiv.org/abs/1009.4353))
- Blinnikov S. I., Eastman R., Bartunov O. S., Popolitov V. A., Woosley S. E., 1998, *ApJ*, **496**, 454
- Blinnikov S. I., Röpke F. K., Sorokina E. I., Gieseler M., Reinecke M., Travaglio C., Hillebrandt W., Stritzinger M., 2006, *A&A*, **453**, 229
- Brayton R., Gustavson F., Hachtel G., 1972, *Proceedings of the IEEE*, **60**, 98
- Brown P. J., et al., 2014, *ApJ*, **787**, 29
- Chakradhari N. K., Sahu D. K., Srivastav S., Anupama G. C., 2014, *MNRAS*, **443**, 1663
- Chevalier R. A., Irwin C. M., 2011, *ApJ*, **729**, L6
- Childress M., et al., 2011, *ApJ*, **733**, 3
- Chugai N. N., et al., 2004, *MNRAS*, **352**, 1213
- Dhawan S., Leibundgut B., Spyromilio J., Blondin S., 2016, *A&A*, **588**, A84
- Dilday B., et al., 2012, *Science*, **337**, 942
- Eastman R. G., Pinto P. A., 1993, *ApJ*, **412**, 731
- Friend D. B., Castor J. I., 1983, *ApJ*, **272**, 259
- Fryer C. L., et al., 2010, *ApJ*, **725**, 296
- Gal-Yam A., et al., 2009, *Nature*, **462**, 624
- Gal-Yam A., et al., 2014, *Nature*, **509**, 471
- Gear C. W., 1971, Numerical initial value problems in ordinary differential equations. Prentice-Hall
- Hachinger S., Mazzali P. A., Taubenberger S., Fink M., Pakmor R., Hillebrandt W., Seitenzahl I. R., 2012, *MNRAS*, **427**, 2057
- Harries T. J., 2015, *MNRAS*, **448**, 3156
- Hauschildt P. H., Baron E., 2004, *A&A*, **417**, 317
- Hicken M., Garnavich P. M., Prieto J. L., Blondin S., DePoy D. L., Kirshner R. P., Parrent J., 2007, *ApJ*, **669**, L17
- Hillebrandt W., Sim S. A., Röpke F. K., 2007, *A&A*, **465**, L17
- Hillier D. J., Dessart L., 2012, *MNRAS*, **424**, 252
- Hillier D. J., Miller D. L., 1998, *ApJ*, **496**, 407
- Hoeflich P., Khokhlov A., 1996, *ApJ*, **457**, 500
- Howell D. A., et al., 2006, *Nature*, **443**, 308

- Kamiya Y., Tanaka M., Nomoto K., Blinnikov S. I., Sorokina E. I., Suzuki T., 2012, *ApJ*, **756**, 191
- Kasen D., Bildsten L., 2010, *ApJ*, **717**, 245
- Kasen D., Thomas R. C., Nugent P., 2006, *ApJ*, **651**, 366
- Kerzendorf W. E., Sim S. A., 2014, *MNRAS*, **440**, 387
- Khan R., Stanek K. Z., Stoll R., Prieto J. L., 2011, *ApJ*, **737**, L24
- Khokhlov A., Mueller E., Hoefflich P., 1993, *A&A*, **270**, 223
- Kromer M., Sim S. A., 2009, *MNRAS*, **398**, 1809
- Kurucz R., 1993, Atomic data for opacity calculations. Kurucz CD-ROM No. 1. Cambridge, Mass.: Smithsonian Astrophysical Observatory, 1993., 1
- LeVeque R. J., 2002, Finite-Volume Methods for Hyperbolic Problems. Cambridge, UK: Cambridge University Press
- Lowrie R. B., Morel J. E., Hittinger J. A., 1999, *ApJ*, **521**, 432
- Maeda K., Kawabata K., Li W., Tanaka M., Mazzali P. A., Hattori T., Nomoto K., Filippenko A. V., 2009, *ApJ*, **690**, 1745
- Mihalas D., Mihalas B. W., 1984, Foundations of Radiation Hydrodynamics. New York: Oxford University Press
- Moll R., Raskin C., Kasen D., Woosley S. E., 2014, *ApJ*, **785**, 105
- Nicholl M., et al., 2013, *Nature*, **502**, 346
- Noebauer U. M., Sim S. A., Kromer M., Röpke F. K., Hillebrandt W., 2012, *MNRAS*, **425**, 1430
- Noebauer U., et al., 2015, The Astronomer's Telegram, **7219**, 1
- Nomoto K., Suzuki T., Deng J., Uenishi T., Hachisu I., 2005, in Turatto M., Benetti S., Zampieri L., Shea W., eds, Astronomical Society of the Pacific Conference Series Vol. 342, 1604-2004: Supernovae as Cosmological Lighthouses. p. 105 ([arXiv:astro-ph/0603432](https://arxiv.org/abs/astro-ph/0603432))
- Nozawa T., Maeda K., Kozasa T., Tanaka M., Nomoto K., Umeda H., 2011, *ApJ*, **736**, 45
- Ofek E. O., et al., 2007, *ApJ*, **659**, L13
- Oran E. S., Boris J. P., 1987, NASA STI/Recon Technical Report A, **88**, 44860
- Pakmor R., Kromer M., Röpke F. K., Sim S. A., Ruiter A. J., Hillebrandt W., 2010, *Nature*, **463**, 61
- Pakmor R., Kromer M., Taubenberger S., Sim S. A., Röpke F. K., Hillebrandt W., 2012, *ApJ*, **747**, L10
- Pfannes J. M. M., Niemeyer J. C., Schmidt W., Klingenberg C., 2010a, *A&A*, **509**, A74
- Pfannes J. M. M., Niemeyer J. C., Schmidt W., 2010b, *A&A*, **509**, A75
- Piro A. L., Morozova V. S., 2016, *ApJ*, **826**, 96
- Raskin C., Kasen D., Moll R., Schwab J., Woosley S., 2014, *ApJ*, **788**, 75
- Roth N., Kasen D., 2015, *ApJS*, **217**, 9
- Scalzo R. A., et al., 2010, *ApJ*, **713**, 1073
- Scalzo R. A., et al., 2014, *MNRAS*, **445**, 30
- Schlegel E. M., 1990, *MNRAS*, **244**, 269
- Sekora M. D., Stone J. M., 2010, *Journal of Computational Physics*, **229**, 6819
- Shen K. J., Bildsten L., Kasen D., Quataert E., 2012, *ApJ*, **748**, 35
- Silverman J. M., Ganeshalingam M., Li W., Filippenko A. V., Miller A. A., Poznanski D., 2011, *MNRAS*, **410**, 585
- Silverman J. M., et al., 2013, *ApJS*, **207**, 3
- Sorokina E., Blinnikov S., 2016, in preparation
- Sorokina E., Blinnikov S., Nomoto K., Quimby R., Tolstov A., 2016, *ApJ*, **829**, 17
- Taubenberger S., et al., 2011, *MNRAS*, **412**, 2735
- Taubenberger S., et al., 2013, *MNRAS*, **432**, 3117
- Webbink R. F., 1984, *ApJ*, **277**, 355
- Wollaeger R. T., van Rossum D. R., 2014, *ApJS*, **214**, 28
- Wollaeger R. T., van Rossum D. R., Graziani C., Couch S. M., Jordan IV G. C., Lamb D. Q., Moses G. A., 2013, *ApJS*, **209**, 36
- Woosley S. E., Kasen D., Blinnikov S., Sorokina E., 2007, *ApJ*, **662**, 487
- Yamanaka M., et al., 2009, *ApJ*, **707**, L118
- Yoon S.-C., Langer N., 2005, *A&A*, **435**, 967